

Heavy Quark Effective Theory at one-loop order: An explicit example



Martin Kurth^a Rainer Sommer^b

^a *Department of Physics and Astronomy, University of Southampton
Southampton SO17 1BJ, UK*

^b *Deutsches Elektronen-Synchrotron, DESY
Platanenallee 6, D-15738 Zeuthen, Germany*

Abstract

We consider correlation functions containing the axial current of one light and one heavy quark in the static approximation as well as in full QCD, using the lattice regularization. Up to one-loop order of perturbation theory, we study the difference between the full and the effective theory in the continuum limit. In the full theory we find a term non-analytic in $1/m$, revealing the asymptotic character of the $1/m$ -expansion. In general, deviations from the $m \rightarrow \infty$ limit turn out to be small and are well described by the first non-trivial terms when m is a factor 2-3 above the external scale. We also investigate the mass dependence of discretization errors, and find that the behaviour of the correlation functions at finite lattice spacing differs significantly from that in the continuum limit when the quark mass is large.

Key words: heavy quark effective theory; matching; lattice QCD

PACS: 11.15.Ha; 12.38.Bx; 12.38.Gc; 12.39.Hg

1 Introduction

Heavy quark effective theory (HQET) is an important tool for heavy quark phenomenology. As a means of decoupling the light degrees of freedom from the mass and spin of heavy quarks (with masses that are much larger than Λ_{QCD}), it is a powerful method to calculate e.g. the heavy hadron spectrum and weak decay form factors. For a review of HQET see [1]. An interesting object to study is the axial current of one light and one heavy quark, as the B-meson decay constant f_B is defined by a matrix element of such a current.

QCD matrix elements have to be evaluated non-perturbatively, which means that the lattice regularization has to be used. As only finite volumes can be treated numerically, and the volume must be large enough to accommodate the physical system such that finite size effects are negligible, current computing power enforces a lower bound on accessible lattice spacings, i.e. an upper bound on the cutoff. As, on today's computers, this cutoff cannot be chosen much larger than the b quark mass, the simulation of bottom flavoured particles is not possible in full QCD, and the use of effective theories like HQET becomes a necessity.

In a previous paper [2], we presented the outline of a method for the non-perturbative renormalization of the heavy-light axial current in the static approximation, which corresponds to the leading order in the heavy quark expansion, where we used Schrödinger functional techniques. In this framework, one considers QCD in a finite volume of linear size L and suitable boundary conditions. The length scale L takes over the rôle played by external momenta p_μ in transition amplitudes in infinite volume. HQET emerges in the large mass limit at fixed L . When no other scale is present, as it is the case in perturbation theory, one has to consider the $z \rightarrow \infty$ limit with $z = mL$ and some definition of the heavy quark mass, m . The predictive power of HQET comes from the fact that the matching of QCD and HQET does not depend on the external states (momenta). It is therefore also independent of the boundary conditions imposed (and L). For this reason we may use the Schrödinger functional to study the relation between the static approximation and full QCD. The advantage is that on the one hand gauge invariant, infrared finite correlation functions may be computed in perturbation theory (rather easily) and on the other hand its lattice-regulated version is very well suited for non-perturbative Monte Carlo simulations [3].

In this paper, we investigate the difference between the static approximation and full QCD in the *continuum* limit, for the specific correlation functions defined in [2], both at tree level and at one-loop order of perturbation theory. For the first time (to our knowledge), it is explicitly demonstrated that gauge invariant, infrared finite correlation functions are described by HQET

in the limit $m \rightarrow \infty$. Indeed, we observe that the $1/m$ -expansion is only an asymptotic expansion; small non-analytic terms $\exp(-z)$ are present in the full theory.

A second point we look at in this paper is the mass dependence of discretization errors, after applying Symanzik's improvement programme [4] to actions, boundary fields, and the axial current.

We use the notation of reference [2]. This paper is organized as follows. In section 2, the basic definitions of the static quark action, both in the continuum and on the lattice, are given. Schrödinger functional boundary conditions and the correlation functions we use are also explained in that section. In section 3, the renormalization schemes we use in the static approximation and in full QCD are introduced. The investigation of finite mass effects, i.e. the difference between the full and effective theories, is carried out in section 4. Section 5 is devoted to the study of discretization errors and their dependence on the heavy quark mass. Our results are summarized in section 6. An appendix contains the relevant one-loop Feynman diagrams.

2 Correlation functions

2.1 Static quarks

Static quarks can be treated as two-component objects. To simplify the notation, they will be described as four-component spinors here, satisfying the constraint

$$P_+ \psi_h = \psi_h, \quad \bar{\psi}_h P_+ = \bar{\psi}_h, \quad P_+ = \frac{1}{2}(1 + \gamma_0). \quad (2.1)$$

The static quark action is

$$S_h = \int d^4x \bar{\psi}_h(x) D_0 \psi_h(x). \quad (2.2)$$

Following [5], we discretize the static quark action as

$$S_h = a^4 \sum_x \bar{\psi}_h(x) \nabla_0^* \psi_h(x). \quad (2.3)$$

2.2 The Schrödinger functional

The Schrödinger functional consists of a finite space-time volume $T \times L \times L \times L$, with specifically chosen boundary conditions. Explicitly, the gauge field is chosen to be periodic in space and to satisfy Dirichlet boundary conditions in time,

$$A_k(x)|_{x_0=0} = C(\mathbf{x}), \quad A_k(x)|_{x_0=T} = [\mathbb{P}C'](\mathbf{x}), \quad (2.4)$$

where $C(\mathbf{x})$ and $C'(\mathbf{x})$ are fixed boundary fields, and \mathbb{P} projects onto the gauge invariant content of $C'(\mathbf{x})$ (see [6]). Here we choose $C = C' = 0$, leading to the boundary conditions

$$U(x, k)|_{x_0=0} = 1, \quad U(x, k)|_{x_0=T} = 1 \quad (2.5)$$

for the lattice gauge field.

The light quark field is chosen to be periodic up to a phase in the three space directions,

$$\psi(x + L\hat{k}) = e^{i\theta}\psi(x), \quad \bar{\psi}(x + L\hat{k}) = \bar{\psi}(x)e^{-i\theta}, \quad (2.6)$$

where θ is kept as a free parameter.

As for the gauge field, Dirichlet boundary conditions are imposed on the light quark field,

$$P_+\psi_1(x)|_{x_0=0} = \rho_1(\mathbf{x}), \quad P_-\psi_1(x)|_{x_0=T} = \rho_1'(\mathbf{x}), \quad (2.7)$$

and

$$\bar{\psi}_1(x)P_-|_{x_0=0} = \bar{\rho}_1(\mathbf{x}), \quad \bar{\psi}_1(x)P_+|_{x_0=T} = \bar{\rho}_1'(\mathbf{x}), \quad (2.8)$$

as well as on the static quark field,

$$\psi_h(x)|_{x_0=0} = \rho_h(\mathbf{x}), \quad \bar{\psi}_h(x)|_{x_0=T} = \bar{\rho}_h'(\mathbf{x}). \quad (2.9)$$

Note that no projectors are necessary in the heavy quark case because of eq. (2.1). For the same reason, we have $P_-\psi_h(x) = 0$. Spatial boundary conditions do not need to be discussed for the static quarks since they do not propagate in space. The quark field boundary conditions given above can be applied both in the continuum and on the lattice.

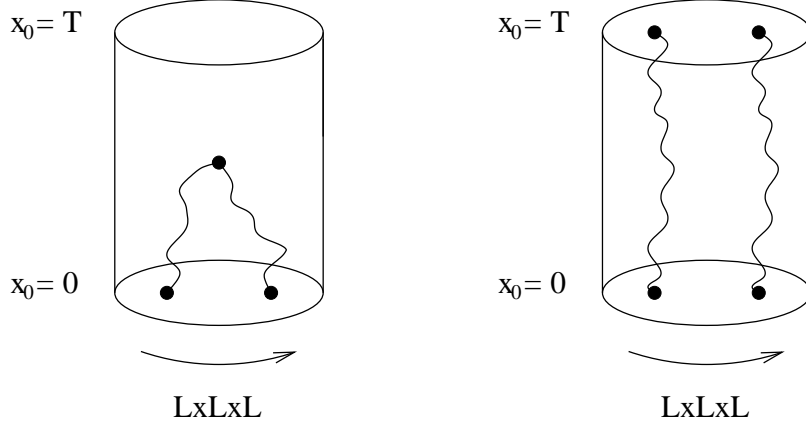


Fig. 1. Schematic drawing of the correlation functions f_A (left) and f_1 (right). The dot in the middle of the left diagram symbolizes the axial current at x_0 , the other dots represent the boundary quark fields.

The Schrödinger functional action, including boundary and $O(a)$ improvement terms, can be found in [6,7,2]. In this paper, it is understood that all quantities are calculated using the $O(a)$ improved action.

2.3 Correlation functions

In the following, we study two different correlation functions. The function f_A contains the time component of a static-light axial current

$$A_0^{\text{stat}}(x) = \bar{\psi}_1(x) \gamma_0 \gamma_5 \psi_h(x) \quad (2.10)$$

or a light-light axial current

$$A_0(x) = \bar{\psi}_1(x) \gamma_0 \gamma_5 \psi_2(x), \quad (2.11)$$

where the indices 1 and 2 label two flavours of relativistic quarks. It is correlated with a suitable combination of “boundary quark fields” to yield the diagram illustrated in the left of Figure 1 upon Wick-contraction. In addition a boundary-to-boundary correlation f_1 , shown on the right of the figure is needed.

With the boundary quark fields $\zeta, \bar{\zeta}$ (see [2] for their proper definition), the correlation functions

$$f_A^{\text{stat}}(x_0) = -\frac{1}{2} \int d^3\mathbf{y} d^3\mathbf{z} \langle A_0^{\text{stat}}(x) \bar{\zeta}_h(\mathbf{y}) \gamma_5 \zeta_1(\mathbf{z}) \rangle \quad (2.12)$$

and

$$f_1^{\text{stat}} = -\frac{1}{2L^6} \int d^3\mathbf{u} d^3\mathbf{v} d^3\mathbf{y} d^3\mathbf{z} \langle \bar{\zeta}_1'(\mathbf{u}) \gamma_5 \zeta_h'(\mathbf{v}) \bar{\zeta}_h(\mathbf{y}) \gamma_5 \zeta_1(\mathbf{z}) \rangle \quad (2.13)$$

can be introduced as in [2]. In addition, the corresponding functions in full QCD,

$$f_A(x_0) = -\frac{1}{2} \int d^3\mathbf{y} d^3\mathbf{z} \langle A_0(x) \bar{\zeta}_2(\mathbf{y}) \gamma_5 \zeta_1(\mathbf{z}) \rangle, \quad (2.14)$$

and

$$f_1 = -\frac{1}{2L^6} \int d^3\mathbf{u} d^3\mathbf{v} d^3\mathbf{y} d^3\mathbf{z} \langle \bar{\zeta}_1'(\mathbf{u}) \gamma_5 \zeta_2'(\mathbf{v}) \bar{\zeta}_2(\mathbf{y}) \gamma_5 \zeta_1(\mathbf{z}) \rangle \quad (2.15)$$

are used. They are discretized as in references [8,9], including $O(a)$ improvement terms

$$ac_A^{\text{stat}} \delta A_0^{\text{stat}} = ac_A^{\text{stat}} \bar{\psi}_1 \frac{1}{2} (\overleftarrow{\nabla}_j + \overleftarrow{\nabla}_j^*) \gamma_j \gamma_5 \psi_h \quad (2.16)$$

and

$$ac_A \delta A_0 = ac_A \frac{1}{2} (\partial_0^* + \partial_0) \{ \bar{\psi}_1 \gamma_5 \psi_2 \}, \quad (2.17)$$

with the improvement coefficients

$$c_A^{\text{stat}} = g_0^2 c_A^{\text{stat}(1)} + O(g_0^4), \quad c_A^{\text{stat}(1)} = -\frac{1}{4\pi} \times 1.00(1) \quad (2.18)$$

and

$$c_A = g_0^2 c_A^{(1)} + O(g_0^4), \quad c_A^{(1)} = -0.00567(1) C_F, \quad (2.19)$$

where the coefficient $c_A^{\text{stat}(1)}$ has been calculated in [10] using NRQCD (a calculation using a different method can be found in [11]), and the coefficient $c_A^{(1)}$ has been taken from [12].

With these correlation functions, the ratios

$$X_1(g_0, L/a) = \frac{f_A^{\text{stat}, I}(T/2)}{\sqrt{f_1^{\text{stat}}}} \quad (2.20)$$

and

$$Y_I(g_0, z, L/a) = \frac{f_A^I(T/2)}{\sqrt{f_1}} \quad (2.21)$$

are defined, where the index I means that the $O(a)$ improved axial currents are used, and z parametrizes the mass dependence as defined in subsection 3.1 below. In the ratios X_I and Y_I , renormalization constants for the light and static quark boundary fields cancel as well as a $1/a$ divergence due to a heavy quark mass counterterm in the static approximation (see [2] for details).

For our perturbative analysis, we expand the ratios to one-loop order,

$$X_I(g_0, L/a) = X_I^{(0)}(L/a) + X_I^{(1)}(L/a)g_0^2 + O(g_0^4), \quad (2.22)$$

$$Y_I(g_0, z, L/a) = Y_I^{(0)}(z, L/a) + Y_I^{(1)}(z, L/a)g_0^2 + O(g_0^4). \quad (2.23)$$

3 Renormalization and matching

When taking the continuum limit, renormalization of quark masses, couplings, and composite operators is required. Bare lattice quark masses m_0 need an additive renormalization

$$m_q = m_0 - m_c \quad (3.1)$$

due to the chiral symmetry breaking term in the Wilson fermion action, defining a reduced quark mass m_q . The critical mass m_c is determined by the requirement that in the case of two mass-degenerate quarks the PCAC mass is zero at $m_q = 0$. In perturbation theory, the critical mass can be expanded as

$$m_c = g_0^2 m_c^{(1)} + O(g_0^4). \quad (3.2)$$

Depending on the precise definition of the PCAC mass, m_c (and therefore also $m_c^{(1)}$) depend on the lattice spacing. However, in perturbation theory one may take the limit where external momentum scales are small compared to the cutoff $1/a$, and extrapolate the coefficient $m_c^{(1)}$ to its continuum limit. This gives [12]

$$am_c^{(1)} = -0.2025565(1) \times C_F, \quad (3.3)$$

a value which will be used also in Sect. 5 at finite values of a . Throughout this paper, we use $m_q = 0$ for the light quark field ψ_1 .

3.1 Renormalization schemes

Unlike the case of full QCD, which is known to be renormalizable at all orders of lattice perturbation theory [13], renormalizability of the static theory has not yet been proven. However, a large number of calculations has been performed in the static approximation, and none of these has given a reason to doubt renormalizability. Throughout this paper, we assume that the static theory is renormalizable “as usual” by adding local counterterms to action and composite fields.

At one-loop level, the ratio X is divergent in the continuum limit, i.e. a scale dependent renormalization is required. The one-loop coefficient $X^{(1)}$ is expected to diverge logarithmically, and a renormalization scheme, the *lattice MS scheme* can be defined by subtracting this logarithm,

$$X_{\text{lat}}(\mu) = Z_{\text{A,lat}}^{\text{stat}}(\mu) X_{\text{I}}(a/L), \quad (3.4)$$

$$Z_{\text{A,lat}}^{\text{stat}}(\mu) = 1 - \gamma_0 \ln(a\mu) g_{\text{lat}}^2, \quad (3.5)$$

where

$$g_{\text{lat}}^2 = g_0^2 + \mathcal{O}(g_0^4), \quad (3.6)$$

and μ is the renormalization scale. The one-loop anomalous dimension of the static axial current

$$\gamma_0 = -\frac{1}{4\pi^2} \quad (3.7)$$

does not depend on the renormalization scheme and is known from [14,15].

The ratio $Y_1(z, a/L)$ remains finite in the continuum limit as long as the coupling and the heavy quark mass are made finite by renormalization. The renormalization condition used here is that, in the continuum limit, they equal the $\overline{\text{MS}}$ coupling and quark masses respectively, at the renormalization scale $1/L$. At one-loop level, this means that the renormalized quantities

$$g_{\overline{\text{MS}}}^2 = g_0^2 + \mathcal{O}(g_0^4) \quad (3.8)$$

and

$$\overline{m}_{2,\overline{\text{MS}}} = Z_{m,\overline{\text{MS}}}(1 + ab_m m_{q,2})m_{q,2} \quad (3.9)$$

are used, where $m_{q,2}$ is the reduced quark mass of the second quark flavour (remember that the mass of the first flavour is chosen to be zero),

$$Z_{m,\overline{\text{MS}}} = 1 - \left(\frac{1}{2\pi^2} \ln(a/L) - 0.122282C_F \right) g_{\overline{\text{MS}}}^2 + \mathcal{O}(g_{\overline{\text{MS}}}^4) \quad (3.10)$$

is known from [16], and the improvement coefficient

$$b_m = -\frac{1}{2} - 0.07217(2)C_F g_0^2 + \mathcal{O}(g_0^4) \quad (3.11)$$

has been calculated in [9].

Taking the continuum limit means to send the lattice spacing to zero while keeping the physical box size fixed. One must thus take the limit $\frac{a}{L} \rightarrow 0$, while $g_{\overline{\text{MS}}}$ and $z = L\overline{m}_{2,\overline{\text{MS}}}$ are kept at fixed values.

A finite renormalization of the light-light axial current is possible, and we define a renormalized current $(A_{\text{CA}})_0$ by requiring that it satisfies the current algebra relations in the case $z = 0$ (see [17,8]). This renormalization condition, together with the $\overline{\text{MS}}$ definition of the coupling and the quark mass, gives a renormalized ratio

$$Y_{\text{CA}}(z, a/L) = Z_A(1 + \frac{1}{2}ab_A m_{q,2})Y_1, \quad (3.12)$$

with the perturbative renormalization constant [16]

$$Z_A = 1 - Z_A^{(1)}C_F g_0^2 + \mathcal{O}(g_0^4), \quad Z_A^{(1)} = -0.0873435, \quad (3.13)$$

and the improvement coefficient [9]

$$b_A = 1 + 0.11414(4)C_F g_0^2 + \mathcal{O}(g_0^4). \quad (3.14)$$

In principle, Y_{CA} should be considered also as a function of $g_{\overline{\text{MS}}}^2$. Since at 1-loop order the dependence on the coupling is rather trivial, we have not indicated it explicitly.

3.2 Matching of full and effective theories

By construction, the effective theory is expected to describe the physics of full QCD in the limit $m \rightarrow \infty$, when this limit is taken appropriately [18]. Beyond the classical level this physics boundary condition translates into a *matching condition* for the two theories, fixing a renormalization scheme (“match”) for the effective theory. The details of the matching conditions should of course be irrelevant, as long as they fix the renormalization constants. To match the axial current, we choose the condition

$$X_{\text{match}}(\overline{m}_{2,\overline{\text{MS}}}) = Y_{\text{CA}}(z, a/L) + \text{O}(1/z) + \text{O}((a/L)^2), \quad (3.15)$$

which means that the effective theory and full QCD are matched at the scale $\mu = \overline{m}_{2,\overline{\text{MS}}}$.

The renormalized static axial current in this scheme is related to the current in the lattice MS scheme by finite renormalization, i. e.

$$X_{\text{match}}(\mu) = (\chi_{\text{A}}^{\text{stat}}) X_{\text{lat}}(\mu) + \text{O}((a/L)^2), \quad (3.16)$$

with

$$(\chi_{\text{A}}^{\text{stat}}) = 1 + B_{\text{A}}^{\text{stat}} g_{\text{lat}}^2 + \text{O}(g_{\text{lat}}^4), \quad (3.17)$$

where $B_{\text{A}}^{\text{stat}}$ is a finite constant. Using

$$\begin{aligned} X_{\text{lat}}^{(1)}(\overline{m}_{2,\overline{\text{MS}}}) &= X_{\text{lat}}^{(1)}(z/L) \\ &= X_{\text{lat}}^{(1)}(1/L) - \gamma_0 \ln(z) X^{(0)}(a/L) + \text{O}((a/L)^2), \end{aligned} \quad (3.18)$$

this constant can be calculated from the matching condition eq. (3.15),

$$\begin{aligned} B_{\text{A}}^{\text{stat}} X^{(0)}(a/L) &= Y_{\text{CA}}^{(1)}(z, a/L) - X_{\text{lat}}^{(1)}(1/L) + \gamma_0 \ln(z) X^{(0)}(a/L) \\ &\quad + \text{O}(1/z) + \text{O}((a/L)^2). \end{aligned} \quad (3.19)$$

Here it is understood that all quantities are extrapolated to the continuum limit first, and then the extrapolation to $1/z = 0$ is performed to determine $B_{\text{A}}^{\text{stat}}$. In practical terms, we define a quantity $\hat{B}_{\text{A}}^{\text{stat}}(z)$ as the continuum limit of

$$\hat{B}_{\text{A}}^{\text{stat}}(z, a/L) = \gamma_0 \ln(z) + \frac{1}{X^{(0)}(a/L)} \left\{ Y_{\text{I}}^{(1)}(z, a/L) \right.$$

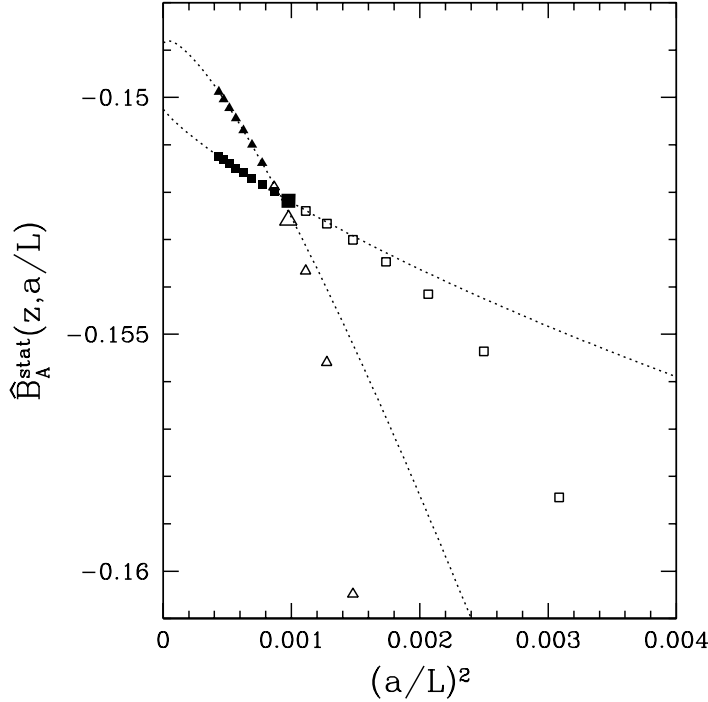


Fig. 2. $\hat{B}_A^{\text{stat}}(z, a/L)$ at $\theta = 0.5$, for $z = 8$ (squares) and $z = 12$ (triangles). The bigger symbols are the data for $L/a = 32$.

$$+ Z_A^{(1)} Y^{(0)}(z, a/L) - X_{\text{lat}}^{(1)}(a/L) \}. \quad (3.20)$$

The continuum limit of $X^{(1)}$ and $Y^{(1)}$ is calculated separately by fitting the numerical data with a function of the expected form [19]

$$\begin{aligned} & h_0 + h_1 \frac{1}{l^2} + h_2 \frac{1}{l^2} \ln(1/l) \\ & + h_3 \frac{1}{l^3} + h_4 \frac{1}{l^3} \ln(1/l) + O(1/l^4), \quad l = L/a, \end{aligned} \quad (3.21)$$

using the fit procedure described in reference [20]. This reference also explains a method to estimate the errors of the fit parameters, which we used in our calculations. For $\theta = 0.5$, we used eq. (3.21) without the $O((a/L)^3)$ terms for $z > 5$ and included those terms in all other fits. For some parameters, the \hat{B}_A^{stat} values resulting from our numerical data and the fits are shown in Fig. 2.

It is expected that

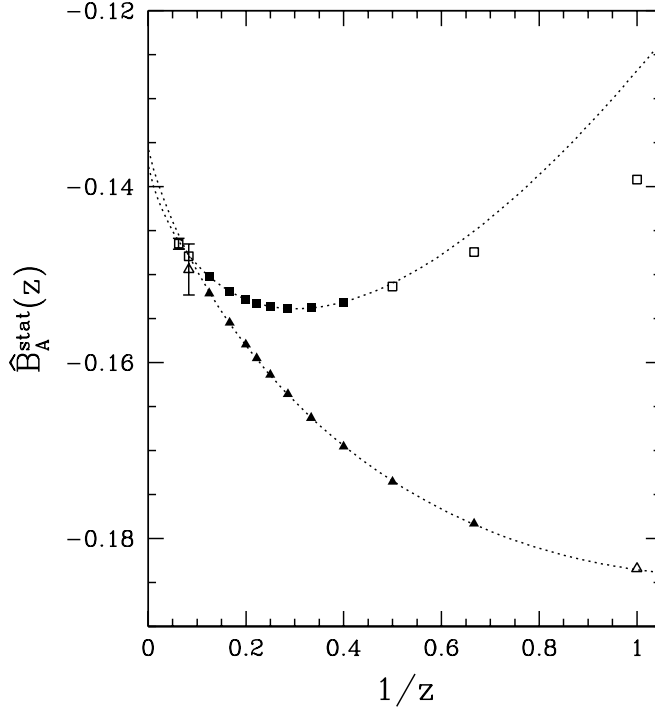


Fig. 3. Calculation of the matching coefficient B_A^{stat} by extrapolation to $1/z = 0$ for $\theta = 0.0$ (triangles) and $\theta = 0.5$ (squares). Where not indicated the errors are smaller than the symbol sizes.

$$\hat{B}_A^{\text{stat}}(z) = B_A^{\text{stat}} + \hat{f}_1 \frac{1}{z} + \hat{f}_2 \frac{1}{z} \ln\left(\frac{1}{z}\right) + O\left(\frac{1}{z^2}\right), \quad (3.22)$$

where $O(1/z^2)$ means terms of the form $1/z^2$ and $\ln(z)/z^2$, and the constants \hat{f}_1 and \hat{f}_2 can be determined from a fit to the numerical data. Figure 3 shows the data for a set of values of z between 1 and 12 at $\theta = 0.0$ and between 1 and 16 at $\theta = 0.5$, as well as fits of the form (3.22), where only the filled symbols have been included in the fits. The results for the fit constants are

θ	B_A^{stat}	\hat{f}_1	\hat{f}_2
0.0	-0.136(3)	-0.05(2)	-0.04(2)
0.5	-0.137(1)	0.011(5)	-0.054(5)

which means that our final result for B_A^{stat} is

$$B_A^{\text{stat}} = -0.137(1). \quad (3.23)$$

This constant is already known from [21], where it has been calculated from matrix elements between quark states, using a gluon mass as infrared regulator. Extracting the relevant terms from that calculation, one gets

$$B_A^{\text{stat}} = -0.14, \quad (3.24)$$

in agreement with our result.

It is more illuminating to turn this logic around: If we take the matching constant B_A^{stat} from matrix elements between quark states, the correlation functions calculated from the static effective theory are the infinite mass limits of the corresponding correlation functions in full QCD, and the mass-dependence of the QCD correlation functions at one loop level has the form expected from HQET. To our knowledge this is the first explicit demonstration of this fact for gauge invariant, infrared finite correlation functions.

4 Heavy quark expansion as an asymptotic series — finite mass effects

As X_{match} is defined by matching to Y_{CA} , the static theory and QCD with relativistic quarks can be compared directly, when these two renormalization schemes are used. To calculate the actual size of the finite mass effects, i.e. the difference between the ratio Y_{CA} and the static limit, we define

$$\Delta(z) = \frac{Y_{\text{CA}}(z) - X_{\text{match}}(\overline{m}_2, \overline{\text{MS}})}{X_{\text{match}}(\overline{m}_2, \overline{\text{MS}})}, \quad (4.1)$$

and expand

$$\Delta(z) = \Delta^{(0)}(z) + \Delta^{(1)}(z)g_{\overline{\text{MS}}}^2 + \mathcal{O}(g_{\overline{\text{MS}}}^4). \quad (4.2)$$

At tree level, the continuum limits of $X^{(0)}$ and $Y^{(0)}$ can be calculated analytically,

$$X^{(0)}(a/L) = -\sqrt{\frac{3\omega_1}{2R_1}}(1 + e^{-\omega_1\tau}) + \mathcal{O}((a/L)^2), \quad (4.3)$$

$$Y^{(0)}(z, a/L) = \frac{1}{\sqrt{2\omega_2 R_2}} \{ (z + \omega_2) + (z - \omega_2)e^{-\omega_2\tau} \} X^{(0)}(a/L)$$

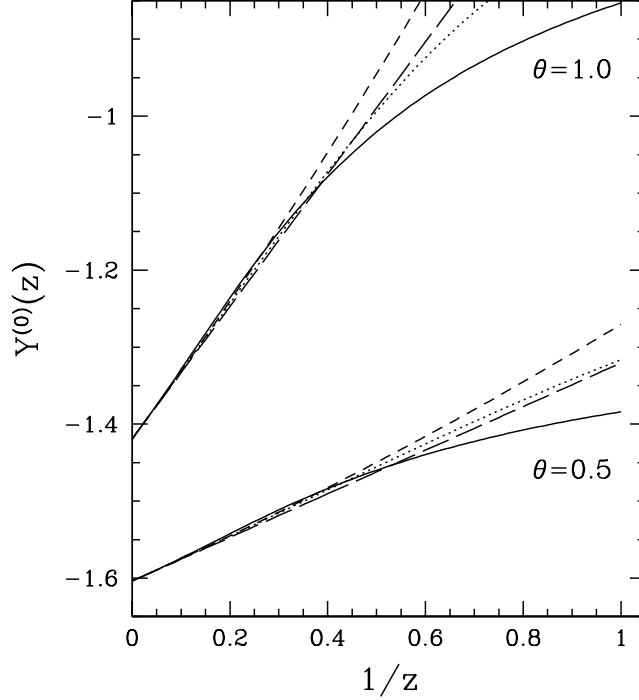


Fig. 4. $Y(z)$ at tree level (solid curve), for $T = L$ and two values of θ , with the expansion up to order $1/z$ (long dashes), order $(1/z)^2$ (short dashes), and order $(1/z)^3$ (dotted curve).

$$+\frac{3\sqrt{3}\theta^2}{2\sqrt{\omega_1\omega_2 R_1 R_2}}(1 - e^{-\omega_1\tau})(1 - e^{-\omega_2\tau}) + O((a/L)^2), \quad (4.4)$$

where

$$\tau = \frac{T}{L}, \quad \omega_1 = \sqrt{3}\theta, \quad \omega_2 = \sqrt{z^2 + 3\theta^2}, \quad (4.5)$$

$$R_1 = \omega_1(1 + e^{-2\omega_1\tau}), \quad R_2 = z + \omega_2 - (z - \omega_2)e^{-2\omega_2\tau}. \quad (4.6)$$

Eq. (4.4) shows that the continuum limit of $Y^{(0)}$ is non-analytic in $1/z$, which means that an expansion in $1/z$ in the sense of a convergent Taylor series is not possible, the expansion is at most asymptotic. However, the non-analytic terms in eq. (4.4) are suppressed by terms of the form $e^{-\omega_2 T}$, and in the static limit $z \rightarrow \infty$, the ratio $Y^{(0)}$ equals the ratio $X^{(0)}$ calculated from the static quark action eq. (2.2). While $Y^{(0)}(z) = X^{(0)}$ for $\theta = 0$, there are finite mass

effects for other values of θ . For $\theta = 0.5$ and $\theta = 1.0$ the resulting curves for $Y^{(0)}$ as a function of $1/z$ are shown in Fig. 4, together with the expansion up to order $(1/z)^3$. The $1/z \rightarrow 0$ limit of these plots gives the respective value of $X^{(0)}$. It is clearly visible that the heavy quark expansion breaks down for $z < 2$, which corresponds to $\overline{m}_{2,\overline{\text{MS}}} < 2/L$.

From eq. (4.3) and eq. (4.4), we get the tree level quantity $\Delta^{(0)}$. The result at $T = L$ is that the finite mass effects for $z \geq 1$ are in the range of 0–14 per cent for $\theta = 0.5$ and 0–40 per cent for $\theta = 1.0$. Details can be read off from Fig. 4.

At one-loop level, the correlation functions are evaluated numerically as described above, and $\Delta^{(1)}(z)$ is calculated from the numerical data shown in Fig. 3. For the set of parameters used in Fig. 3, $\Delta^{(1)}$ lies between 0 and 5 per cent for $\theta = 0.0$, and between 0 and 2 per cent for $\theta = 0.5$.

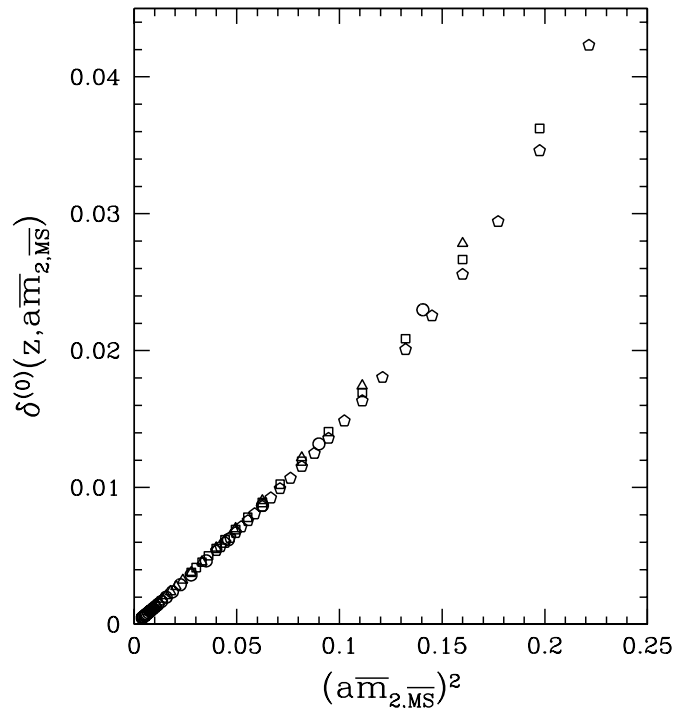


Fig. 5. Discretization errors in the ratio $Y(z)$ at tree level. The circles are $z = 3$ data, the triangles $z = 4$, the squares $z = 8$, and the pentagons $z = 16$.

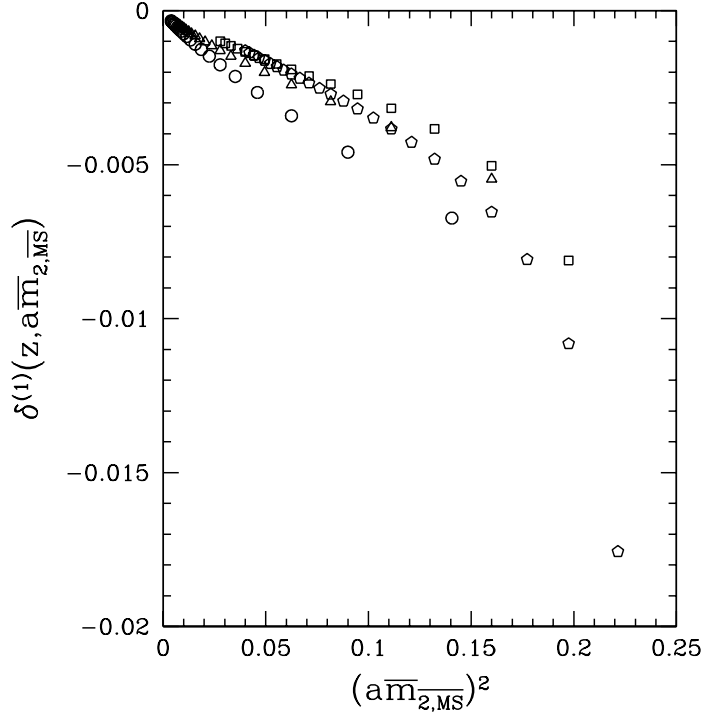


Fig. 6. Discretization errors in the ratio $Y(z)$ at one-loop level. The circles are $z = 3$ data, the triangles $z = 4$, the squares $z = 8$, and the pentagons $z = 16$.

5 Cutoff effects

As we use an $O(a)$ improved action, improved boundary fields, and improved operators in our lattice calculation, we expect discretization errors of $O(a^2)$. These are expected to depend on the heavy quark mass. To shed some light on the mass dependence of the discretization errors, we define

$$\delta(z, a\bar{m}_{2,\overline{\text{MS}}}) = \frac{Y_{\text{CA}}(z, a/L) - Y_{\text{CA}}(z, 0)}{Y_{\text{CA}}(z, 0)}, \quad (5.1)$$

and expand again,

$$\delta = \delta^{(0)} + \delta^{(1)}g_{\overline{\text{MS}}}^2 + O(g_{\overline{\text{MS}}}^4). \quad (5.2)$$

We calculate $\delta^{(0)}$ and $\delta^{(1)}$ for a range of different values of z and a/L , and print them as a function of $(a\bar{m}_{2,\overline{\text{MS}}})^2$ in Fig. 5 and Fig. 6. The figures show that (for our choice of parameters) the discretization errors are roughly proportional

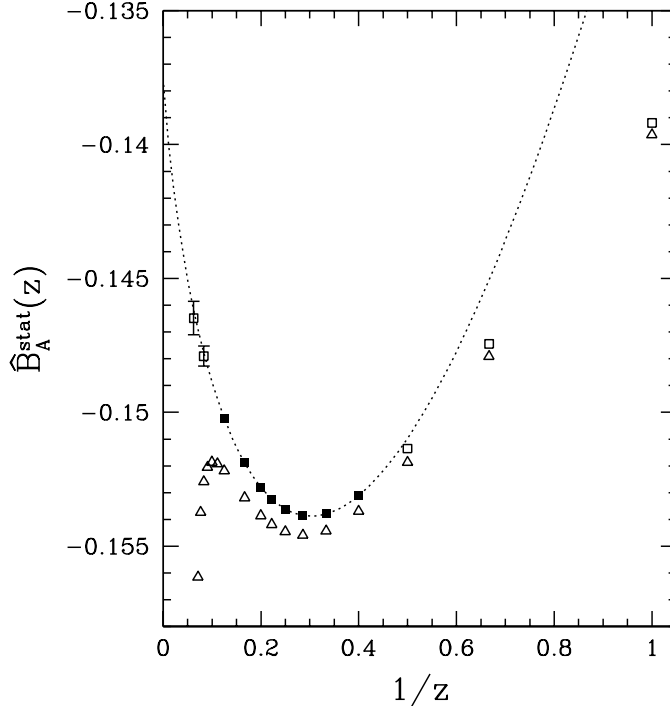


Fig. 7. The matching coefficient \hat{B}_A^{stat} in the continuum limit (squares) and at $L/a = 32$ (triangles) for $\theta = 0.5$. The dotted line is the fit explained in Sect. 3.

to $(a\bar{m}_{2,\overline{\text{MS}}})^2$. This is a significant problem in heavy quark extrapolations at finite lattice spacing, as due to the mass dependence of the discretization errors, there is a certain risk that the slope being used in the extrapolation contains a sizeable contribution from discretization errors. To illustrate this a bit further, Fig. 7 shows the quantity \hat{B}_A^{stat} introduced in Sect. 3, both in the continuum with the fit described above, and at finite lattice spacing $L/a = 32$. Here again it can be seen that the discretization errors increase with the value of the heavy quark mass, and for $z > 8$ (which means $a\bar{m}_{2,\overline{\text{MS}}} > 1/4$) the behaviour of the curve at finite lattice spacing changes dramatically. That this is really due to a cutoff effect can be seen from Fig. 2, where the data points for $L/a = 32$ have been marked by slightly bigger symbols. This shows that $O(a)$ improvement breaks down for too large values of $a\bar{m}_{2,\overline{\text{MS}}}$, and heavy quark extrapolations should be performed in the continuum limit rather than at finite lattice spacing. A detailed explanation of the improvement breakdown for heavy quarks can be found in section 4 of ref. [22], where this effect is discussed in the context of the Schrödinger functional renormalization of the QCD gauge coupling.

A comparison between the values of $\delta(z, a\overline{m}_{2,\overline{\text{MS}}})$ for $a\overline{m}_{2,\overline{\text{MS}}} < 1/2$ and $\Delta(z)$ for $z \geq 2$, both at tree and one-loop level, shows that the discretization errors and the finite mass effects are of comparable size, i.e. of the order of a few per cent.

6 Conclusions

The main point of this paper is a comparison between the axial current in QCD with finite quark masses, and in the static approximation at one-loop order of perturbation theory. To achieve this, we have defined gauge invariant, infrared finite, finite-volume correlation functions with Schrödinger functional boundary conditions, and constructed ratios of these correlation functions to cancel renormalization constants except for that of the axial current. Furthermore, the divergence due to the residual mass term in the static theory cancels in our ratios.

Using these ratios, and assuming renormalizability of the static theory, we have defined a renormalization scheme for the static-light axial current by matching to the full theory, such that the renormalized static ratio equals the heavy-quark limit of the corresponding ratio calculated from full QCD. This renormalization scheme allows a comparison between the full and the static theory. Taking the matching constant B_A^{stat} from one specific matching condition, we have verified explicitly that the heavy quark limit of an independent correlation function is described by HQET. For quark masses down to $1/L$, where L is the extent of the space-time box, the finite-mass effects in our ratio are in the range of a few per cent, both at tree level and at one-loop order of perturbation theory.

As we performed our calculations in the lattice regularization, we were also able to investigate discretization errors in our ratio of correlation functions, both at tree and one-loop level. We have shown that (for our choice of parameters), the tree level and one-loop coefficients approach the continuum limit at a rate roughly proportional to $(am)^2$, if $O(a)$ improvement is applied to the action, the boundary fields, and to composite operators. We observe a significant difference between continuum limit data and results at finite lattice spacing, with a qualitative difference in the behaviour of the two curves for $am > 1/4$. This demonstrates that extrapolations in the heavy quark mass should be carried out in the continuum limit rather than at finite lattice spacings.

Acknowledgement

We thank F. Jegerlehner for useful comments on the manuscript.

A Feynman diagrams

The expansion of the correlation functions f_A and f_1 is described in detail in ref. [12]. Following that method, we get the one-loop Feynman diagrams shown in Fig. A.1 and Fig. A.2.

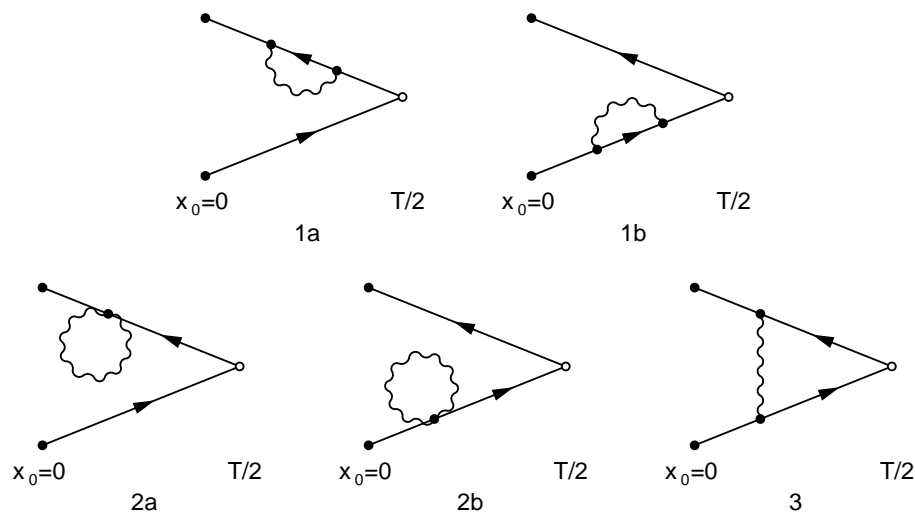


Fig. A.1. One loop diagrams contributing to $f_A(T/2)$.

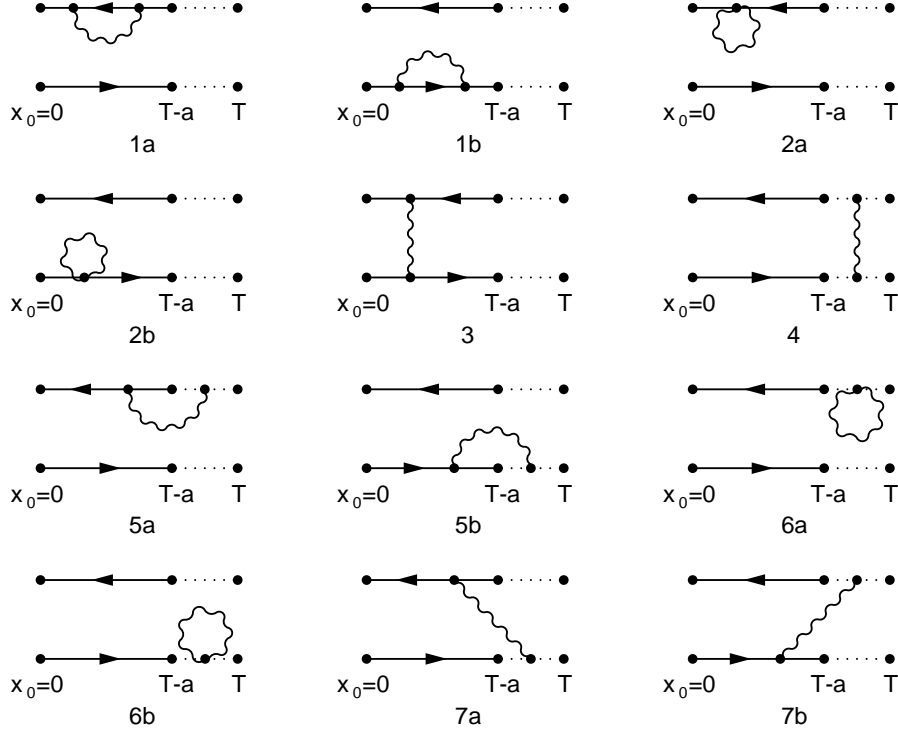


Fig. A.2. One loop diagrams contributing to f_1 . The dotted lines denote the link from $T - a$ to T .

References

- [1] M. Neubert, Phys. Rept. 245 (1994) 259, hep-ph/9306320, and references therein.
- [2] ALPHA, M. Kurth and R. Sommer, Nucl. Phys. B597 (2001) 488, hep-lat/0007002.
- [3] K. Jansen et al., Phys. Lett. B372 (1996) 275, hep-lat/9512009.
- [4] K. Symanzik, Nucl. Phys. B226 (1983) 187.
- [5] E. Eichten and B. Hill, Phys. Lett. B234 (1990) 511.
- [6] M. Lüscher, R. Narayanan, P. Weisz and U. Wolff, Nucl. Phys. B384 (1992) 168, hep-lat/9207009.
- [7] S. Sint, Nucl. Phys. B421 (1994) 135, hep-lat/9312079.
- [8] M. Lüscher, S. Sint, R. Sommer and H. Wittig, Nucl. Phys. B491 (1997) 344, hep-lat/9611015.
- [9] S. Sint and P. Weisz, Nucl. Phys. B502 (1997) 251, hep-lat/9704001.

- [10] C. Morningstar and J. Shigemitsu, Phys. Rev. D57 (1998), hep-lat/9712015.
- [11] K.I. Ishikawa, T. Onogi and N. Yamada, Nucl. Phys. Proc. Suppl. 83 (2000) 301, hep-lat/9909159.
- [12] M. Lüscher and P. Weisz, Nucl. Phys. B479 (1996) 429, hep-lat/9606016.
- [13] T. Reisz, Nucl. Phys. B318 (1989) 417.
- [14] M.A. Shifman and M.B. Voloshin, Sov. J. Nucl. Phys. 45 (1987) 292.
- [15] H.D. Politzer and M.B. Wise, Phys. Lett. B206 (1988) 681.
- [16] E. Gabrielli, G. Martinelli, C. Pittori, G. Heatlie and C.T. Sachrajda, Nucl. Phys. B362 (1991) 475.
- [17] M. Bochicchio, L. Maiani, G. Martinelli, G.C. Rossi and M. Testa, Nucl. Phys. B262 (1985) 331.
- [18] T. Mannel, W. Roberts and Z. Ryzak, Nucl. Phys. B368 (1992) 204.
- [19] M. Lüscher and P. Weisz, Nucl. Phys. B266 (1986) 309.
- [20] ALPHA, A. Bode, P. Weisz and U. Wolff, Nucl. Phys. B576 (2000) 517, hep-lat/9911018.
- [21] A. Borrelli and C. Pittori, Nucl. Phys. B385 (1992) 502.
- [22] S. Sint and R. Sommer, Nucl. Phys. B465 (1996) 71, hep-lat/9508012.